Synthesis of High-Density, Large-Diameter, and Aligned Single-Walled Carbon Nanotubes by Multiple-Cycle Growth Methods

Weiwei Zhou, Lei Ding, Sungwoo Yang, and Jie Liu*

Department of Chemistry, Duke University, Durham, North Carolina 27708, United States

ABSTRACT A dense array of parallel single-walled carbon nanotubes (SWNTs) as the device channel can carry higher current, be more robust, and have smaller device-to-device variation, thus is more desirable for and compatible with applications in future highly integrated circuits when compared with single-tube devices. The density of the parallel SWNT arrays and the diameter of SWNTs both are key factors in the determination of the device performance. In this paper, we present a new multiple-cycle chemical vapor deposition (CVD) method to synthesize horizontally aligned arrays of SWNTs with densities of 20−40 SWNT/μm over large area and a diameter distribution of 2.4 $\pm$ 0.5 nm on the quartz surface based on a methanol/ethanol CVD method. The high nucleation efficiency of catalyst particles in multiple-cycle CVD processes has been demonstrated to be the main reason for the improvements in the density of SWNT arrays. More interestingly, we confirmed the existence of an etching effect, which strongly affects the final products in the multiple-cycle growth. This etching effect is likely the reason that only large-diameter SWNTs were obtained in the multiple-cycle CVD growth. Using these high-density and large-diameter nanotube arrays, two-terminal devices with back-gates were fabricated. The performances of these devices have been greatly improved in overall resistance and on-state current, which indicates these SWNT arrays have high potential for applications such as interconnects, high-frequency devices, and high-current transistors in future micro- or nanoelectronics.

KEYWORDS: single-walled carbon nanotubes · single-crystal quartz · horizontally aligned arrays · high density · large diameter

Since the resistance of a copper wire greatly increases with a decrease in size,[1] carbon nanotubes have been proposed as more suitable candidates for the narrow-line-width interconnects in future circuits for their higher current-carrying capability and ballistic transport property.[2−5] However, a single-walled carbon nanotube (SWNT), as a one-dimensional (1D) molecular wire, has relatively high quantum resistance, which limited their further application in the micro- and nanoelectronic industry.[4] Theoretical analysis[6−8] and experimental results[5,9−14] both have demonstrated that due to the obvious improvements in the on-driving current, mobility, and cutoff frequency, a dense parallel SWNT array has more advantages for the scalable fabrication of highly integrated circuits, especially for high-frequency electronics where impedance matching becomes important.[4] On the other hand, earlier studies showed current-carrying capability differences between different SWNTs can be more than 2 orders of magnitude[15−17] depending on their diameters. In addition, SWNTs with a diameter larger than 1.4 nm have been reported to form better contact with metals having high work functions such as Pd and Au.[16] Moreover, simulations show carriers in large-diameter SWNTs exhibit higher mobilities at low field and have a good potential for realizing ballistic transport.[18−20] Therefore, large-diameter SWNTs are more desirable for fabricating reliable SWNT-based interconnects and logic devices.

In summary, an ideal strategy to optimize the performance of SWNT-based interconnects and logic devices is to have both high density and large diameters in SWNT arrays. In recent years, chemical vapor deposition (CVD) methods have shown rapid progress in the growth of perfectly aligned SWNTs on single crystal wafers such as quartz[21−27] and sapphire.[28−30] Especially, the density of the aligned SWNT arrays synthesized on Y-cut quartz substrates can be as high as 60 SWNTs/μm,[24] which has never been achieved on silicon wafer or sapphire. In addition, SWNTs synthesized on quartz have very narrow diameter distributions. For example, SWNTs with 1.1 $\pm$ 0.4 and 1.2 $\pm$ 0.3 nm diameter distributions were obtained on quartz substrates by using methane[23] and ethanol[24] as carbon feeding stocks, respectively. We also found that introducing methanol and ethanol together into the growth process can shift the

* Address correspondence to j.liu@duke.edu.

Received for review January 18, 2011 and accepted March 31, 2011.

Published online March 31, 2011
10.1021/nn200198b

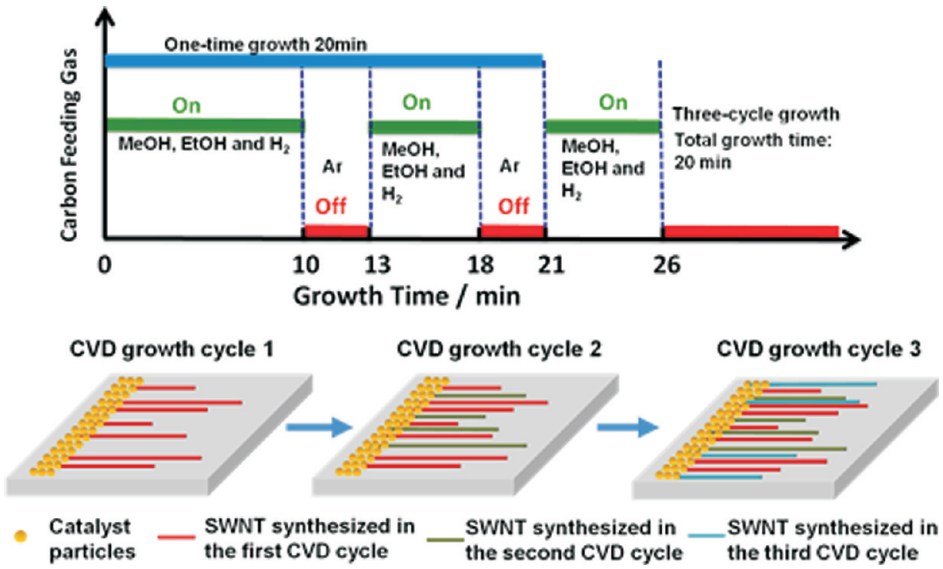

Scheme 1. Strategy and experimental process illustrations of growing a horizontally aligned SWNT array on quartz substrate by three-cycle CVD growth.

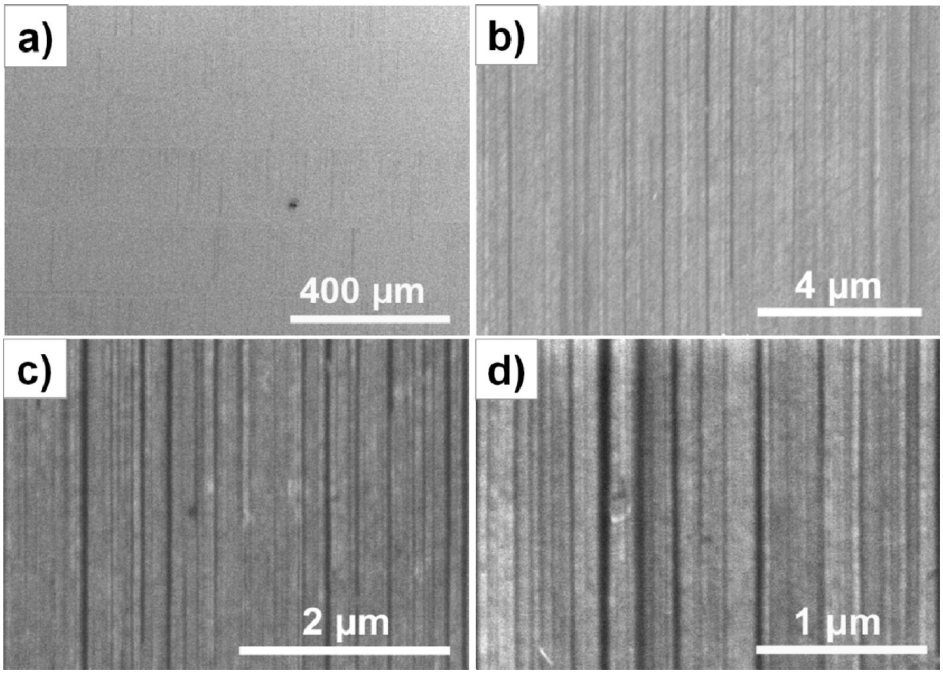

Figure 1. SEM images with different magnifications of a horizontally aligned array of SWNTs with highly dense packing on single-crystal quartz surface after a typical three-cycle methanol/ethanol CVD growth.

average SWNT diameter from 1.2 to 1.65 nm.[25] Therefore, methanol/ethanol CVD is currently the best option to grow large-diameter SWNTs on quartz substrates. However, the typical density of SWNT arrays made by this method is ~5 SWNT/μm,[25] although in some areas the density can be as high as 20 SWNT/μm.[31] However, the uniformity of the sample is not satisfactory.

In the paper, we demonstrate a new multiple-cycle CVD method to successfully synthesize ultra-high-density and large-diameter arrays of SWNTs over large areas and with high uniformity on the quartz surface. The growth conditions of multiple-cycle growth are similar to the methanol/ethanol CVD method,[25] but the carbon precursor feedstock was stopped for a short period intermittently (shown in Scheme 1). After a typical three-cycle growth, we found that the density of the nanotube arrays can be improved to 20–40 SWNTs/μm, which is 3–4 times higher than samples made by one-time growth. At the same time, the diameters of SWNTs showed an obvious increase. The distribution is 2.4 $\pm$ 0.5 nm. As a result of the improved density and diameter of SWNTs, the average per-μm-width resistance of the devices made from these arrays

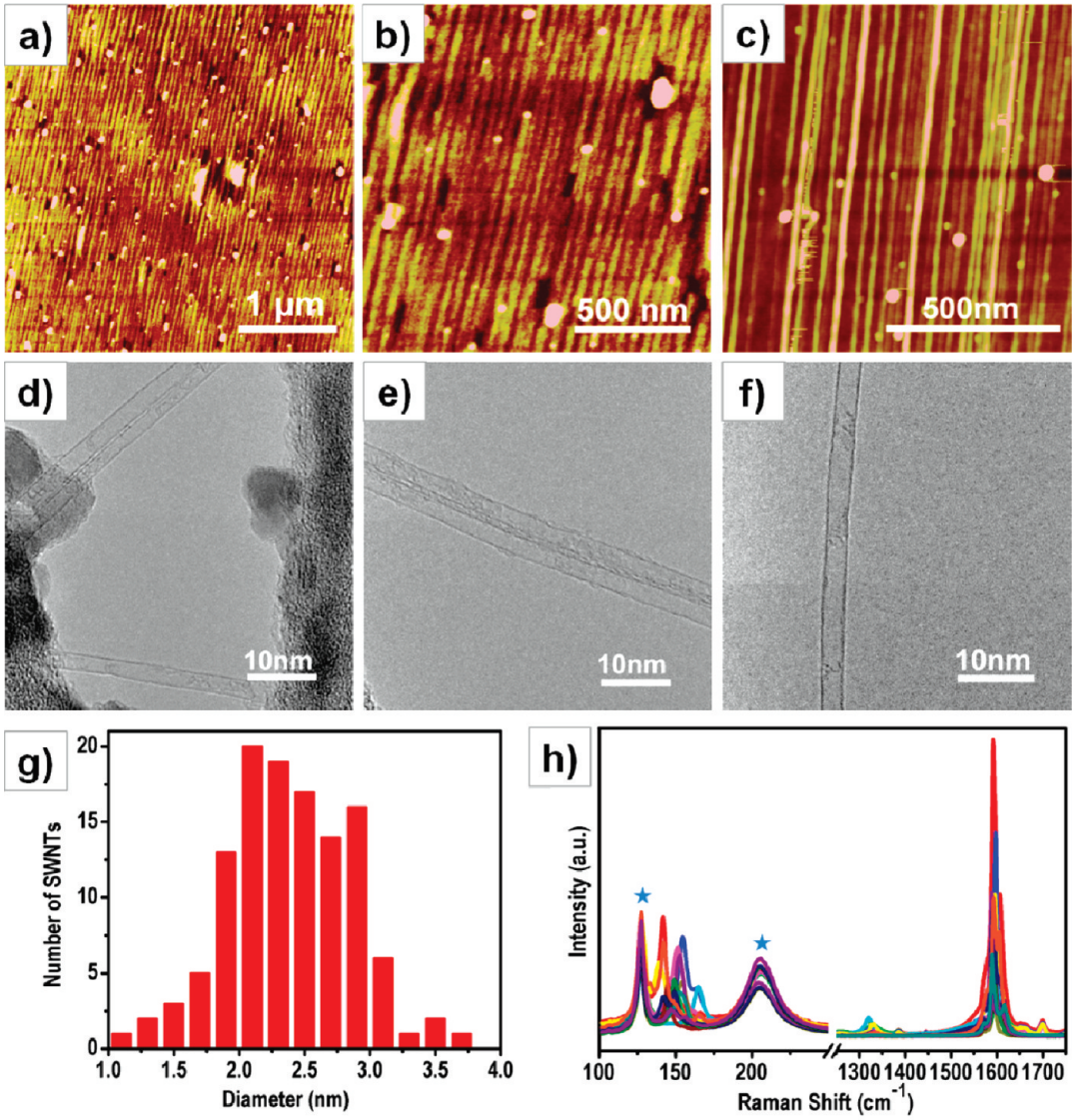

Figure 2. AFM images (a–c) of the sample shown in Figure 1 with a density of 20–40 SWNT/μm. In some areas SWNTs are so close to each other that they form a continual monolayer film. HRTEM images (d–f) and corresponding Raman spectra (h) verified that in this sample SWNTs were synthesized and have large diameters. The Raman spectra were collected from 15 different spots on the sample surface with an excitation laser line of 633 nm. The peaks marked by blue stars in the Raman spectra are sourced from single-crystal quartz substrate. A histogram (g) of diameter distribution of this SWNT array was obtained by measuring over 120 SWNTs from HRTEM images. The average diameter is 2.4 nm, and standard deviation is 0.5 nm.

is ~12 times lower than that of the devices made from SWNT arrays from one-time growth. Furthermore, the on-state current densities of back-gated FETs made from these SWNT arrays are also very high, up to 220 μA/μm. These results not only improved the performances of the fabricated devices but also provided important information on the growth mechanism of carbon nanotubes under a condition where growth and etching processes compete with each other.

RESULTS AND DISCUSSION

The design of the multiple-cycle growth method is motivated by our earlier study on orthogonal growth of nanotubes on Y-cut quartz surface,[32] where we found horizontally aligned SWNTs can grow between nanotube forests in the second CVD process without the need to add new catalysts. This observation indicates that at least part of catalyst particles can keep their catalytic activities even after a CVD growth process. We speculate that these catalysts can be reactivated to nucleate new nanotubes if we somehow restart the growth step. To confirm this hypothesis, we designed and tested multiple CVD growth cycles using the methanol/ethanol CVD method originally used for growing horizontally aligned nanotubes on quartz (Scheme 1). By analyzing SEM and AFM results, we discovered that this three-cycle growth method is a simple but effective way to improve the density of SWNT arrays on quartz wafers.

SEM images (Figure 1) show a horizontally aligned SWNT array with highly dense packing uniformly

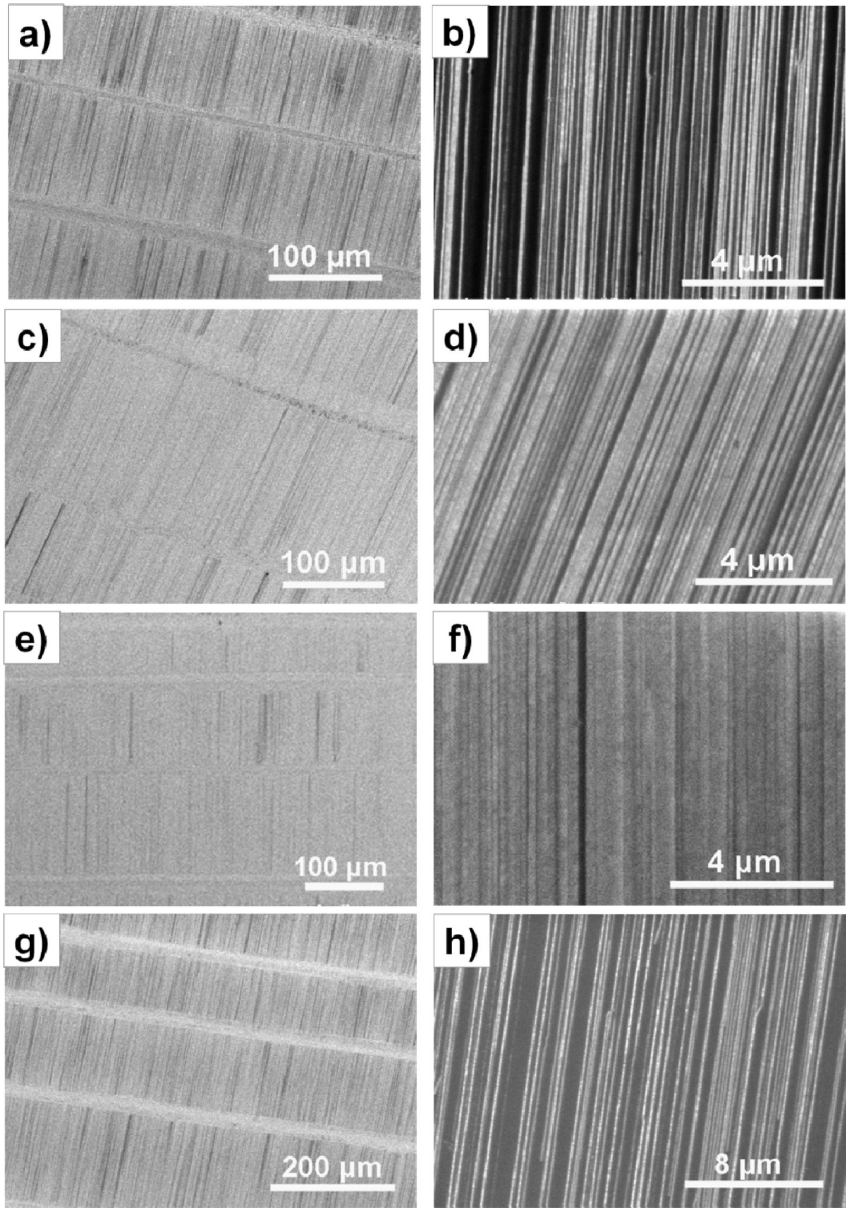

Figure 3. SEM images of horizontally aligned SWNT arrays synthesized on quartz surface by normal one-time growth (a, b), two-cycle growth (c, d), three-cycle growth (e, f), and four-cycle growth (g, h) under the same CVD conditions.

covering the surface after a typical three-cycle CVD growth. The density of the aligned SWNTs is so high that we are not able to measure the density of the SWNT array by SEM. AFM, as a higher resolution tool, was used to further characterize the SWNT arrays. AFM images (Figure 2a−c) show that the density of the array is 20−40 SWNTs/μm. In some areas, SWNTs almost formed a continuous monolayer, and it is hard to distinguish the isolated SWNTs in AFM images (shown in Figure 2a and b). The radial breathing mode (RBM) peaks frequently detected in the low-frequency regime and low peak intensity ratio of the D band over the G band in the Raman spectra (Figure 2h) verified that SWNTs were synthesized on the quartz surface. In order to more accurately measure the diameter of nanotubes, the SWNT array was transferred onto a copper grid for HRTEM characterization. By measuring more than 120 nanotubes, we found the diameter distribution (shown in Figure 2g) is 2.4 $\pm$ 0.5 nm; only three nanotubes have diameters below 1.4 nm, and the minimum size is 1.2 nm. According to HRTEM results (shown in Figure 2d−f), no few-walled carbon nanotubes (FWNTs) can be found even when the nanotube is larger than 3 nm.

Even though an obvious increase in SWNT density has been achieved by the multiple-cycle CVD method, it is necessary and important for us to further investigate the detailed mechanism. Many studies of SWNT growth have shown that a key factor for the high-yield growth of SWNTs is to activate more catalyst particles

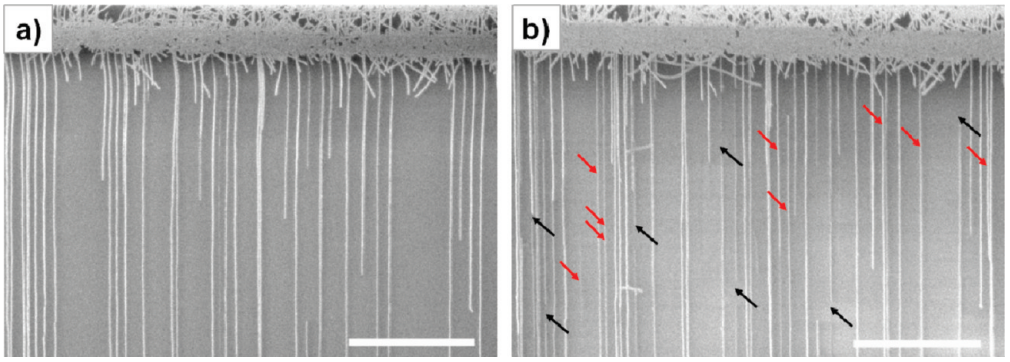

Figure 4. SEM images of SWNTs grown from the same catalyst lines after the first CVD growth (a) and after the second CVD growth (b). The nanotubes marked with red arrows were synthesized in the second CVD growth. The nanotubes marked with black arrows were partially etched in the second CVD growth. The scale bars in both images are 10 μm.

to nucleate SWNTs at the beginning stage of the CVD process.[33−35] For a normal one-time growth, catalyst particles have only one chance to nucleate SWNT, but for a three-cycle growth, catalyst particles have more chances, which means higher probability for these catalysts to be activated. We propose that at the beginning stage of every CVD growth cycle there are always some new catalyst particles starting to grow SWNTs, so the percentage of catalyst particles activated in all three growth cycles is much higher than in one-time growth. To verify our hypothesis, we performed one-time growth, two-cycle growth, and four-cycle growth respectively on different samples and under the same CVD conditions. SEM images (Figure 3) show the density of SWNT arrays gradually increased from 5 to 10 SWNTs/μm for one-time growth to 10−20 SWNTs/μm for two-cycle growth and then reached the highest value (20−40 SWNTs/μm) for three-cycle growth. More nanotubes gradually grew out from catalyst regions. Therefore, multiple-cycle CVD is an effective way to enhance the catalyst efficiency.

In order to further confirm this hypothesis, a controlled experiment comparing the growth results in the same area of the quartz wafer after the first-cycle growth and after the second-cycle growth has been conducted. The sample was taken out from the furnace after the first-cycle growth for SEM characterization and then put back into the furnace for the second growth under the same CVD conditions. Low-density SWNT arrays were synthesized under a chosen CVD condition in this experiment for a better comparison using SEM characterization. As shown in Figure 4b, after the second CVD cycle nine new SWNTs marked with red arrows grew out from the same catalyst area on the wafer after the first CVD growth, which directly verifies that more catalyst particles were activated in multiple-cycle CVD growth. This result is in good agreement with our previous results on orthogonal growth of nanotubes on Y-cut quartz surfaces.

Another interesting phenomenon is that after a four-cycle growth experiment, the density of SWNTs started to decrease and the density is even lower than the one-time growth result. This means many nanotubes were etched away in the fourth CVD cycle. In fact, we have also noticed in Figure 4b that in addition to the growth of nine new nanotubes there are seven existing nanotubes partially etched after the second CVD cycle, which are marked by black arrows. Therefore, we believe there are two simultaneous reactions in the nanotube growth environment, etching and growing, that compete with each other. In the fourth growth cycle, the etching effect starts to dominate over the growth, thus resulting in the decrease of SWNT density. This etching effect has not been carefully studied yet, but we speculate that it is from −OH groups because the oxygen atoms in −OH groups have a weak oxidation function and can react with amorphous carbon.[36−38]

In order to further investigate the etching effect, we changed the three-cycle growth conditions by only stopping ethanol and H_2 flow but keeping methanol/Ar flow as the protecting gas in the off stage between the two CVD growth steps. The results (Figure S1 in the Supporting Information) show that only a limited number of short nanotubes were synthesized, which means methanol has an obvious etching effect on carbon nanotubes at 900 °C and further indicates the −OH group can react with not only amorphous carbon but also carbon nanotubes. Moreover, we believe the etching effect plays a very important role in determining the diameter distribution of SWNTs because small-diameter carbon nanotubes are less stable than large-diameter nanotubes and thus can be preferentially etched by −OH species.[39]

Compared to the one-time growth result, the nanotubes synthesized by three-cycle growth have much larger diameters and higher density, which are more suitable for fabrication of interconnects or transistors in electrical circuits. Figure 5a and b show the layout design and a photo image of a two-terminal device group composed of four devices with a channel length of ~2 μm and with different widths, which are ~5, ~10, ~10, and ~50 μm, respectively. Ten groups (total

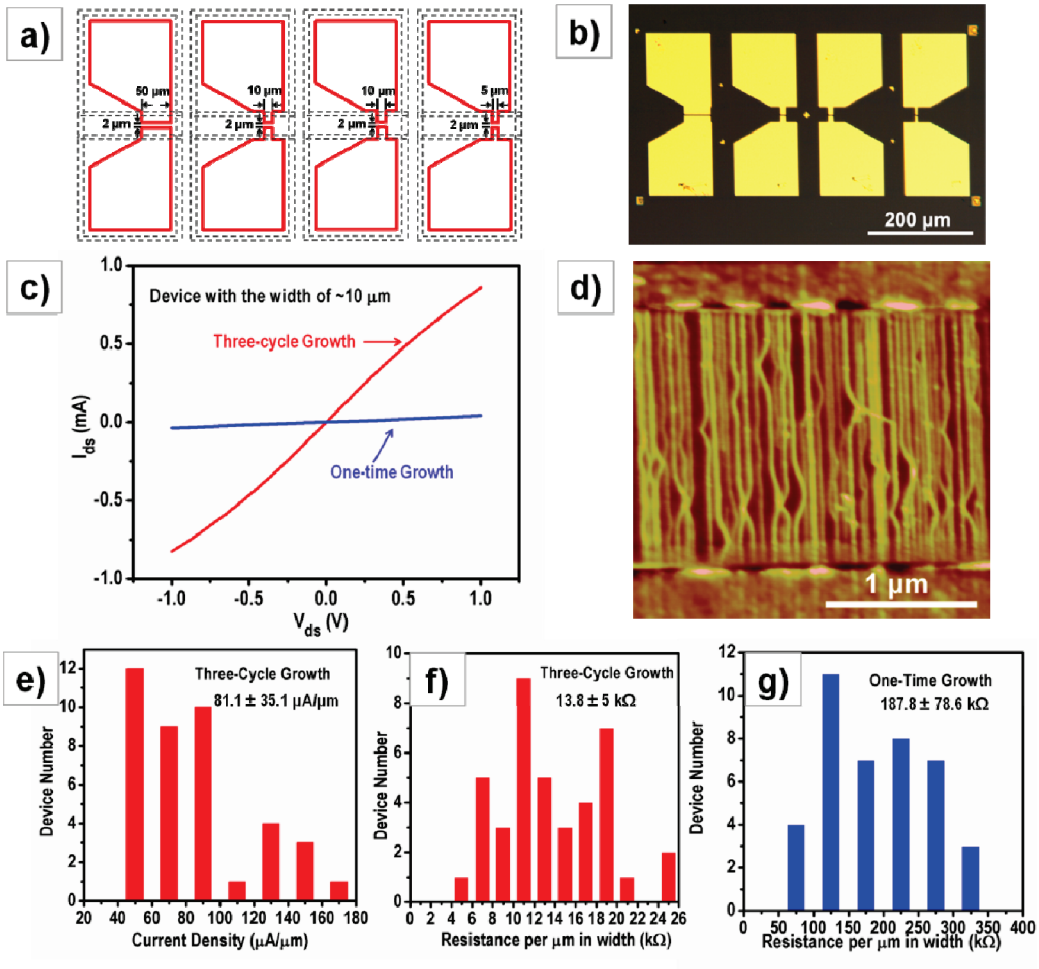

Figure 5. Schematic layout (a) and photo image (b) of a two-terminal device group composed of four devices with the channel length of ~2 μm and the different widths of ~5, ~10, ~10, and ~50 μm, respectively. Ti (1.2 nm)/Pd (20 nm)/Au (40 nm) were used as contact metals. The SWNTs in the dashed line area of (a) were removed by O_2 plasma etching. (c) Current–voltage characteristics of the representative devices with channel widths of ~10 μm made by three-cycle growth sample (red curve) and one-time growth sample (blue curve). (d) Corresponding AFM image of the device in (c). Histograms of output current density distribution (e) and per-μm-in-width resistance distribution (f) of the 40 devices made by a three-cycle growth sample. (g) Histogram of per-μm-in-width resistance distribution of the 40 devices made by a one-time growth sample.

40 devices) were fabricated for more accurately estimating the performances of those devices. The different width electrodes were designed for testing the uniformity of the SWNT array, but we found all devices show very high output current densities and low per-width resistances. The histogram (shown in Figure 5e) obtained by measuring all 40 devices shows that the distribution of output current density at 1 V voltage is 81.1 ± 35.1 μA/μm, with the highest value being 174.1 μA/μm. The AFM image of a representative device with the width of 10 μm and its current–voltage characteristics are shown in Figure 5c and d.

The distribution of the per-μm-in-width resistances for ultra-high-density SWNT array based devices (shown in Figure 5f) is 13.8 ± 5 kΩ, and the lowest observed value in our experiment is 5.7 kΩ. We also measured another 40 devices with the same configurations made by one-time growth samples with a typical density of ~5 SWNT/μm and found the currents are much lower (representative current–voltage characteristics are shown in Figure 5c). The distribution of the per-μm-in-width resistances is shown in Figure 5g. The average value is 187.8 kΩ (shown in Figure 5g), which is ~12 times higher than that of ultra-high-density SWNT array based devices. According to the current–voltage measurement results, the high output current and low resistance are attributed to not only the density increase of 3–4 times but also the diameter increase, which further confirms that a large-diameter carbon nanotube can form better contacts.

At the same time, the performances of FETs based on an ultra-high-density SWNT array also were tested using silicon back-gating. The distribution of on-state current density is 108.9 ± 42.6 μA/μm, and the highest value observed in our experiments is 220 μA/μm (shown in Figure 6c). It is also much higher than the current density of FETs made using a one-time growth

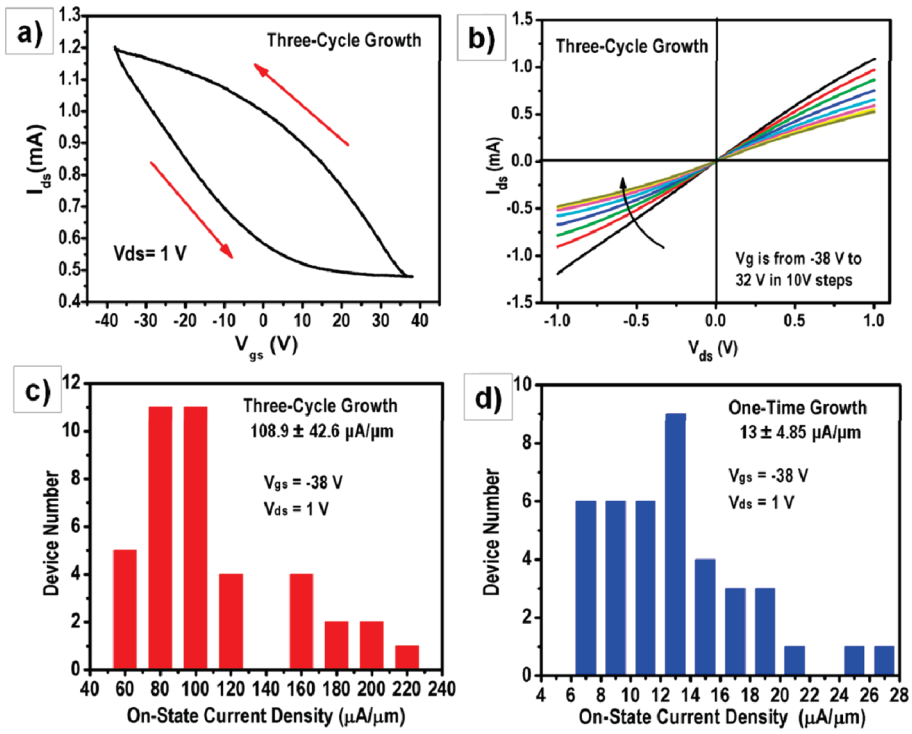

Figure 6. Transfer characteristics (a) and output characteristics (b) of a representative back-gated FET with the channel width of ~10 μm based on the SWNT array synthesized by three-cycle growth. Histograms of on-state current density distributions of the devices based on the SWNT array synthesized by three-cycle growth (c) and the SWNT array with a density of ~5 SWNT/μm synthesized by one-time growth (d). For every histogram, 40 transistors were measured. The currents were measured at V_{gs} = −38 V and V_{ds} = 1 V.

sample. However, the on/off ratios of FET are 2−4 (transfer characteristics of a representative FET are shown in Figure 6a), which is much lower than the one-time growth result previously reported (~20).[25] We also found that the on/off ratio cannot be improved by the electrical breakdown technique even when the on-state current of the devices degraded over 90%. We speculate that this is due to the high percentage of larger diameter SWNTs in the three-cycle growth sample. Although large-diameter SWNTs form a lower Schottky barrier with the contact metal and can carry higher current, the large-diameter-SWNTs-based FETs often showed a low on/off ratio because the large diameter also can result in a large leakage current.[40,41] The detailed reason for the on/off ratio decrease of the device is under further investigation. However, the high current-carrying capability of these aligned large-diameter nanotubes makes them interesting candidates for interconnects in high-frequency devices and antennas.[4]

CONCLUSION

In conclusion, we have successfully synthesized horizontally aligned SWNT arrays with high density and large diameters using multiple-cycle CVD growth. The density is around 20−40 SWNTs/μm. In some regions, SWNTs are very close to each other and almost form a continuous monolayer. HRTEM results verified single-walled carbon nanotubes were synthesized and show the diameter distribution of SWNTs in the array is 2.4 ± 0.5 nm. We attribute the density increase of the SWNT array to the high efficiency of catalyst particles because more catalyst particles can be activated during the multiple CVD cycles, and we further confirm this hypothesis by a comparison of one-, two-, three-, and four-cycle growth results and *in situ* analysis of SEM images of the same catalyst area on a quartz wafer after the first and the second growth. The multiple-cycle CVD growth is a simple but universal method and could be a way to realize highly efficient growth of carbon nanotubes. At the same time, we found etching effect of −OH groups in the multiple-cycle growth, which resulted in the density decrease after four-cycle growth and probably is the reason for selective growth of large-diameter SWNTs in three-cycle growth.

Based on this ultra-high-density and large-diameter SWNT array, two-terminal devices with high output currents and low resistances were fabricated. Using silicon back-gating, transfer characteristics of the devices were measured and show the on-state current density is up to ~220 μA/μm. Very recently, Zhou's group at the University of Southern California showed that aligned-nanotube-based devices with a 0.5 μm channel length exhibited an on-current density of 92.4 μA/μm before removing metallic nanotubes, which was the highest value prior to this work.[27] Although the on/off ratio is lower than the one-time

growth result due to a high percentage of large-diameter nanotubes in the arrays, this highly dense and large-diameter SWNT array has potential as interconnects and antennas in future electronics.

METHODS

Multiple-Cycle CVD Growth Process. The strategy is shown in Scheme 1. In a typical experiment, $CuCl_2$/poly(vinylpyrrolidone) used as catalyst precursor was patterned on Y-cut quartz wafers first following a procedure described previously.[24] The quartz wafers were calcined at 720 °C in air for 20 min to remove photoresist and form Cu_xO_y nanoparticles. After cooling down to room temperature, the furnace was heated to 775 °C and left at 775 °C for 15 min in a H_2 atmosphere, followed by the CVD growth of SWNTs at 900 °C. A flow of hydrogen (360 sccm) and argon (60−75 sccm through an ethanol bubbler and 300 sccm through a methanol bubbler) was introduced into the system for 10 min. Then the furnace was left at 900 °C for 3 min, and high-flow-rate Ar gas (600 sccm) was introduced for flushing the chamber and removing H_2 gas and alcohol vapor. This is the first growth cycle. The next CVD-growth cycle condition is the same as the first cycle, but the growth time was changed to 5 min. Typically, we performed three cycles in a CVD-growth procedure.

Fabrication of the Devices Based on SWNT Arrays. SWNT arrays were transferred onto a silicon wafer with a 100 nm SiO_2 layer before the fabrication of devices following a published precedure.[25] Two-terminal devices are patterned by a standard e-beam lithography (EBL) process. Ti (1.2 nm)/Pd (20 nm)/Au (40 nm) were deposited by e-beam evaporation, followed by a lift-off process to form contact electrodes. Another EBL process and O_2 plasma etching were used to remove the shortening nanotubes outside the device channel region. A back-side Si gate was used for measuring the performances of FETs. A Keithley 4200-SCS semiconductor characterization system was used for measuring the electrical characteristics.

Characterization. A scanning electron microscope (SEM, FEI XL30 S-FEG, operated at 1 or 1.5 kV), an atomic force microscope (AFM, Digital Instruments Multi-Mode SPM Nanoscope IIIa, operated at tapping-mode), a high-resolution transmission electron microscope (HRTEM, Tecnai F20 FEG-TEM, operated at 200 kV), and a micro-Raman spectroscope (Horiba Jobin Yvon LabRam ARAMIS) were used to characterize the produced SWNTs. The excitation wavelength of the micro-Raman is 633 nm. For HRTEM characterization, the samples were transferred from quartz wafers onto the Cu grids.

Acknowledgment. This work was supported in part by a grant from NRL (N00173-04-1-G902) and ONR (N00014-09-1-0163). The authors also acknowledge the Shared Materials Instrumentation Facility at Duke University for access to their instrumentation.

Supporting Information Available: Further experimental details and supportive SEM data. This material is available free of charge *via* the Internet at http://pubs.acs.org.

REFERENCES AND NOTES

1. Rossnagel, S. M.; Kuan, T. S. Alteration of Cu Conductivity in the Size Effect Regime. *J. Vac. Sci. Technol. B* **2004,** *22*, 240–247.
2. Naeemi, A.; Sarvari, R.; Meindl, J. D. Performance Comparison between Carbon Nanotube and Copper Interconnects for Gigascale Integration (GSI). *IEEE Electron Device Lett.* **2005,** *26*, 84–86.
3. Close, G. F.; Yasuda, S.; Paul, B.; Fujita, S.; Wong, H. S. P. A 1 GHz Integrated Circuit with Carbon Nanotube Interconnects and Silicon Transistors. *Nano Lett.* **2008,** *8*, 706–709.
4. Rutherglen, C.; Burke, P. Nanoelectromagnetics: Circuit and Electromagnetic Properties of Carbon Nanotubes. *Small* **2009,** *5*, 884–906.
5. Plombon, J. J.; O'Brien, K. P.; Gstrein, F.; Dubin, V. M.; Jiao, Y. High-Frequency Electrical Properties of Individual and Bundled Carbon Nanotubes. *Appl. Phys. Lett.* **2007,** *90*, 063106.
6. Naeemi, A.; Meindl, J. D. Impact of Electron-Phonon Scattering on the Performance of Carbon Nanotube Interconnects for GSI. *IEEE Electron Device Lett.* **2005,** *26*, 476–478.
7. Naeemi, A.; Meindl, J. D. Monolayer Metallic Nanotube Interconnects: Promising Candidates for Short Local Interconnects. *IEEE Electron Device Lett.* **2005,** *26*, 544–546.
8. Guo, J.; Hasan, S.; Javey, A.; Bosman, G.; Lundstrom, M. Assessment of High-Frequency Performance Potential of Carbon Nanotube Transistors. *IEEE Trans. Nanotechnol.* **2005,** *4*, 715–721.
9. Kang, S. J.; Kocabas, C.; Ozel, T.; Shim, M.; Pimparkar, N.; Alam, M. A.; Rotkin, S. V.; Rogers, J. A. High-Performance Electronics Using Dense, Perfectly Aligned Arrays of Single-Walled Carbon Nanotubes. *Nat. Nanotechnol.* **2007,** *2*, 230–236.
10. Ryu, K.; Badmaev, A.; Wang, C.; Lin, A.; Patil, N.; Gomez, L.; Kumar, A.; Mitra, S.; Wong, H. S. P.; Zhou, C. W. CMOS-Analogous Wafer-Scale Nanotube-on-Insulator Approach for Submicrometer Devices and Integrated Circuits Using Aligned Nanotubes. *Nano Lett.* **2009,** *9*, 189–197.
11. Kocabas, C.; Kim, H. S.; Banks, T.; Rogers, J. A.; Pesetski, A. A.; Baumgardner, J. E.; Krishnaswamy, S. V.; Zhang, H. Radio Frequency Analog Electronics Based on Carbon Nanotube Transistors. *Proc. Natl. Acad. Sci. U. S. A.* **2008,** *105*, 1405–1409.
12. Rutherglen, C.; Jain, D.; Burke, P. Rf Resistance and Inductance of Massively Parallel Single Walled Carbon Nanotubes: Direct, Broadband Measurements and Near Perfect 50 Omega Impedance Matching. *Appl. Phys. Lett.* **2008,** *93*, 083119.
13. Tselev, A.; Woodson, M.; Qian, C.; Liu, J. Microwave Impedance Spectroscopy of Dense Carbon Nanotube Bundles. *Nano Lett.* **2008,** *8*, 152–156.
14. Kocabas, C.; Dunham, S.; Cao, Q.; Cimino, K.; Ho, X. N.; Kim, H. S.; Dawson, D.; Payne, J.; Stuenkel, M.; Zhang, H. *et al* High-Frequency Performance of Submicrometer Transistors That Use Aligned Arrays of Single-Walled Carbon Nanotubes. *Nano Lett.* **2009,** *9*, 1937–1943.
15. Anantram, M. P. Current-Carrying Capacity of Carbon Nanotubes. *Phys. Rev. B* **2000,** *62*, R4837–R4840.
16. Chen, Z. H.; Appenzeller, J.; Knoch, J.; Lin, Y. M.; Avouris, P. The Role of Metal-Nanotube Contact in the Performance of Carbon Nanotube Field-Effect Transistors. *Nano Lett.* **2005,** *5*, 1497–1502.
17. Tseng, Y. C.; Phoa, K.; Carlton, D.; Bokor, J. Effect of Diameter Variation in a Large Set of Carbon Nanotube Transistors. *Nano Lett.* **2006,** *6*, 1364–1368.
18. Pennington, G.; Goldsman, N. Semiclassical Transport and Phonon Scattering of Electrons in Semiconducting Carbon Nanotubes. *Phys. Rev. B* **2003,** *68*, 045426.
19. d'Honincthun, H. C.; Galdin-Retailleau, S.; See, J.; Dollfus, P. Electron-Phonon Scattering and Ballistic Behaviour in Semiconducting Carbon Nanotubes. *Appl. Phys. Lett.* **2005,** *87*, 172112.
20. Kauser, M. Z.; Ruden, P. P. Effects of Chirality and Diameter on the Transport Properties of Semiconducting Carbon Nanotubes. *J. Appl. Phys.* **2007,** *102*, 033712.
21. Kocabas, C.; Hur, S. H.; Gaur, A.; Meitl, M. A.; Shim, M.; Rogers, J. A. Guided Growth of Large-Scale, Horizontally Aligned Arrays of Single-Walled Carbon Nanotubes and Their Use in Thin-Film Transistors. *Small* **2005,** *1*, 1110–1116.
22. Kocabas, C.; Kang, S. J.; Ozel, T.; Shim, M.; Rogers, J. A. Improved Synthesis of Aligned Arrays of Single-Walled Carbon Nanotubes and Their Implementation in Thin Film Type Transistors. *J. Phys. Chem. C* **2007,** *111*, 17879–17886.

23. Zhou, W. W.; Rutherglen, C.; Burke, P. Wafer Scale Synthesis of Dense Aligned Arrays of SWNTs. *Nano Res.* **2008,** *1*, 158–165.
24. Ding, L.; Yuan, D. N.; Liu, J. Growth of High-Density Parallel Arrays of Long Single-Walled Carbon Nanotubes on Quartz Substrates. *J. Am. Chem. Soc.* **2008,** *130*, 5428–5429.
25. Ding, L.; Tselev, A.; Wang, J. Y.; Yuan, D. N.; Chu, H. B.; McNicholas, T. P.; Li, Y.; Liu, J. Selective Growth of Well-Aligned Semiconducting Single-Walled Carbon Nanotubes. *Nano Lett.* **2009,** *9*, 800–805.
26. Hong, S. W.; Banks, T.; Rogers, J. A. Improved Density in Aligned Arrays of Single-Walled Carbon Nanotubes by Sequential Chemical Vapor Deposition on Quartz. *Adv. Mater.* **2010,** *22*, 1826–1830.
27. Wang, C.; Ryu, K.; De-Arco, L. G.; Badmaev, A.; Zhang, J. L.; Lin, X.; Che, Y. C.; Zhou, C. W. Synthesis and Device Applications of High-Density Aligned Carbon Nanotubes Using Low-Pressure Chemical Vapor Deposition and Stacked Multiple Transfer. *Nano Res.* **2010,** *3*, 831–842.
28. Ismach, A.; Segev, L.; Wachtel, E.; Joselevich, E. Atomic-Step-Templated Formation of Single Wall Carbon Nanotube Patterns. *Angew. Chem., Int. Ed.* **2004,** *43*, 6140–6143.
29. Han, S.; Liu, X. L.; Zhou, C. W. Template-Free Directional Growth of Single-Walled Carbon Nanotubes on A- and R-Plane Sapphire. *J. Am. Chem. Soc.* **2005,** *127*, 5294–5295.
30. Ago, H.; Nakamura, K.; Ikeda, K.; Uehara, N.; Ishigami, N.; Tsuji, M. Aligned Growth of Isolated Single-Walled Carbon Nanotubes Programmed by Atomic Arrangement of Substrate Surface. *Chem. Phys. Lett.* **2005,** *408*, 433–438.
31. Ding, L.; Zhou, W. W.; Thomas, P. M.; Wang, J.; Chu, H.; Li, Y.; Liu, J. Direct Observation of the High Affinity Interaction between Carbon Nanotubes and Quartz. *Nano Res.* **2009,** *2*, 903–910.
32. Zhou, W. W.; Ding, L.; Yang, S. W.; Liu, J. Orthogonal Orientation Control of Carbon Nanotube Growth. *J. Am. Chem. Soc.* **2010,** *132*, 336–341.
33. Deng, W. Q.; Xu, X.; Goddard, W. A. A Two-Stage Mechanism of Bimetallic Catalyzed Growth of Single-Walled Carbon Nanotubes. *Nano Lett.* **2004,** *4*, 2331–2335.
34. Futaba, D. N.; Hata, K.; Namai, T.; Yamada, T.; Mizuno, K.; Hayamizu, Y.; Yumura, M.; Iijima, S. 84% Catalyst Activity of Water-Assisted Growth of Single Walled Carbon Nanotube Forest Characterization by a Statistical and Macroscopic Approach. *J. Phys. Chem. B* **2006,** *110*, 8035–8038.
35. Qi, H.; Yuan, D. N.; Liu, J. Two-Stage Growth of Single-Walled Carbon Nanotubes. *J. Phys. Chem. C* **2007,** *111*, 6158–6160.
36. Hata, K.; Futaba, D. N.; Mizuno, K.; Namai, T.; Yumura, M.; Iijima, S. Water-Assisted Highly Efficient Synthesis of Impurity-Free Single-Walled Carbon Nanotubes. *Science* **2004,** *306*, 1362–1364.
37. Yamada, T.; Maigne, A.; Yudasaka, M.; Mizuno, K.; Futaba, D. N.; Yumura, M.; Iijima, S.; Hata, K. Revealing the Secret of Water-Assisted Carbon Nanotube Synthesis by Microscopic Observation of the Interaction of Water on the Catalysts. *Nano Lett.* **2008,** *8*, 4288–4292.
38. Futaba, D. N.; Goto, J.; Yasuda, S.; Yamada, T.; Yumura, M.; Hata, K. General Rules Governing the Highly Efficient Growth of Carbon Nanotubes. *Adv. Mater.* **2009,** *21*, 4811–4815.
39. Zhou, W.; Ooi, Y. H.; Russo, R.; Papanek, P.; Luzzi, D. E.; Fischer, J. E.; Bronikowski, M. J.; Willis, P. A.; Smalley, R. E. Structural Characterization and Diameter-Dependent Oxidative Stability of Single Wall Carbon Nanotubes Synthesized by the Catalytic Decomposition of CO. *Chem. Phys. Lett.* **2001,** *350*, 6–14.
40. Wang, Z. X.; Ding, L.; Pei, T. A.; Zhang, Z. Y.; Wang, S.; Yu, T.; Ye, X. F.; Peng, F.; Li, Y.; Peng, L. M. Large Signal Operation of Small Band-Gap Carbon Nanotube-Based Ambipolar Transistor: A High-Performance Frequency Doubler. *Nano Lett.* **2010,** *10*, 3648–3655.
41. Guo, J.; Datta, S.; Lundstrom, M. A Numerical Study of Scaling Issues for Schottky-Barrier Carbon Nanotube Transistors. *IEEE Trans. Electron Devices* **2004,** *51*, 172–177.